



Effects of raw materials on the electrochemical performance of Na-doped Li-rich cathode materials $\text{Li}[\text{Li}_{0.2}\text{Ni}_{0.2}\text{Mn}_{0.6}]\text{O}_2$

Hongzhao Liu^{1,2} · Lei Tao³ · Wei Wang^{1,2} · Bo Zhang^{1,2} · Mingru Su⁴

Received: 24 May 2018 / Revised: 28 July 2018 / Accepted: 15 August 2018 / Published online: 28 August 2018
© Springer-Verlag GmbH Germany, part of Springer Nature 2018

Abstract

Lithium-ion battery cathode materials $\text{Li}_{1.2}\text{Ni}_{0.2}\text{Mn}_{0.6}\text{O}_2$ and $\text{Li}_{1.15}\text{Na}_{0.05}\text{Ni}_{0.2}\text{Mn}_{0.6}\text{O}_2$ were synthesized using different Na source through a facile ball-milling method. The XRD results reveal that all the cathode materials display a layered structure of solid solution. Charge/discharge tests demonstrate that the $\text{Li}_{1.15}\text{Na}_{0.05}\text{Ni}_{0.2}\text{Mn}_{0.6}\text{O}_2$ electrode using LiAC and NaAC as raw materials shows an excellent electrochemical performance including high reversible discharge capacity (232 mAhg^{-1} at 0.2 C), enhanced rate capability (109 mAhg^{-1} at 5 C), and superior cycling stability (96.64% capacity retention after 80 cycles). Furthermore, EIS results also support that better raw materials can effectively decrease the charge transfer resistance and facilitate the Li diffusion coefficient of the as-prepared cathode material. It is also confirmed that the better electrochemical performance of the Na-doped sample $\text{Li}_{1.15}\text{Na}_{0.05}\text{Ni}_{0.2}\text{Mn}_{0.6}\text{O}_2$ mainly come from the Na-doping process which stabilizes the host layered structure by suppressing the conversion from layered to spinel structure during cycling.

Keywords Lithium-ion battery · Raw materials · Na-doping · Electrochemical performance

Introduction

Today, lithium-ion batteries have achieved a dominant position in the field of energy storage due to their high energy densities and low cost. Lithium-ion batteries are presently being developed as an efficient energy storage device to power cell phones, laptop computers, and hybrid electric vehicles (HEVs and EVs). [1–6] Among the commercial cathode materials, the layered lithium-rich manganese-based cathode materials generally denoted as $x\text{Li}_2\text{MnO}_3 \cdot (1-x)\text{LiMO}_2$ ($M = \text{Ni}$,

Co, Mn, etc.) are considered as an efficient cathode material due to its high reversible capacity and super security. [7–10]

However, there are several major deficiencies which hinder their practical commercialization: low initial coulombic efficiency [11], due to the generation of oxygen vacancies and irreversible capacity loss during the first cycle; poor rate performance [12], attributed to the poor surface conductivity which is caused by the solid electrolyte interface (SEI) film and its low electronic conductivity; and insufficient capacity retention [13], owing to layered to spinel transformation during long-term cycling. To solve these problems, many groups have explored various solutions to improve the electrochemical performance.

The first possible attempt is surface modification [14–18]. It has been found that treatment with acid, persulfate, and $(\text{NH}_4)_2\text{HPO}_4$ can induce the layered to spinel phase transformation. And the paths provided by the spinel structure can accelerate Li ions cross through the surface of cathode materials at high current densities. The second method is surface coating [19]. As reported, a series of compounds have been applied to coat on the cathode materials, such as inert oxides [20, 21], metal phosphate [22, 23], and metal fluoride [24, 25]. Surface coating can form a surface with higher electrical conductivity to improve the poor rate capability. In addition, cation doping is another feasible strategy which can stabilize the crystal structure, resulting in an improvement of the electrochemical

✉ Bo Zhang
zhangboz@163.com

Mingru Su
sumingru@163.com

¹ Zhengzhou Institute of Multipurpose Utilization of Mineral Resources, Zhengzhou 450006, China
² Key Laboratory of Evaluation and Multipurpose Utilization of Polymetallic Ore of Ministry of Land and Resources, Zhengzhou 450006, China
³ Jiangsu GE New Energy Technology Co., Ltd, Yangzhong 212200, China
⁴ School of Material Science and Technology Jiangsu University, Zhenjiang 212013, China

performance. [26–29] Thus far, researchers have successfully introduced a number of cations into the bulk lattice, such as Al, Cr, Zr, and Fe, to replace lithium or substitute the transition metal like Ni, Co, or Mn, leading to an enhancement of the coulombic efficiency and a stable structure.

Considering the efficiency and cost of the various solutions mentioned above, a befitting preparation method is very crucial for the cathode materials. According to the recent reports, a better coulombic efficiency, higher discharge capacity, and enhanced lithium diffusivity have been achieved after introducing cations with similar radius to the Li ion such as Na, K, and Mg into Li sites. In particular, Hu et al. [30] synthesized Na-stabilized Ni-rich $\text{Li}_{1-x}\text{Na}_x\text{Ni}_{0.8}\text{Co}_{0.15}\text{Al}_{0.05}\text{O}_2$ through coprecipitation and the solid-state calcination route. The Guo group [31] synthesized K-doped $\text{Li}_1\text{Ni}_{0.5}\text{Mn}_{0.3}\text{Co}_{0.2}\text{O}_2$ through a substitution of the Li source method and the Wang group [32] synthesized Na-doped $\text{Li}_{1.4}[\text{Mn}_{0.6}\text{Ni}_{0.2}\text{Co}_{0.2}]\text{O}_2$ using a solvothermal method. Though the initial coulombic efficiency and cycle stability of the as-prepared Na-doped lithium-rich cathode materials can be improved to some extent, these Na-doping processes are complex and costly. And to our best knowledge, though it has been found that Na-doping is an effective way to improve the electrochemical performance, the effects of different raw materials on the electrochemical performance and structural stability of the layered lithium-rich Mn-based oxide materials are still lacking quantitative research.

The sodium acetate (300 °C) and sodium carbonate (851 °C) [33] were adopted as the different Na source to synthesize layered Li-rich Mn-based cathode materials $\text{Li}_{1.2}\text{Ni}_{0.2}\text{Mn}_{0.6}\text{O}_2$ and $\text{Li}_{1.15}\text{Na}_{0.05}\text{Ni}_{0.2}\text{Mn}_{0.6}\text{O}_2$, respectively. It is believed that the lower melting point is beneficial for the decomposition and crystallization of the cathode materials. In this paper, Na was introduced into the Li layer via a simple, facile ball-milling method following high-temperature solid state reaction; its microstructure and electrochemical performance were investigated specifically. We also discussed its effect on Li diffusion in detail, which is sensitive to the Li slab distance in the layered materials. What is more, in order to clarify the impact of raw materials on the electrochemistry performance of Na-doped $\text{Li}_{1.2}\text{Ni}_{0.2}\text{Mn}_{0.6}\text{O}_2$ cathode material, we systematically investigate the relationship between the Na source and comprehensive performance of cathode materials, especially the electrochemical property.

Experiment

Synthesis of materials

A simple ball-milling procedure followed by a high temperature solid-state reaction was used for the synthesis of the pristine sample $\text{Li}_{1.2}\text{Ni}_{0.2}\text{Mn}_{0.6}\text{O}_2$ and Na-doped sample

$\text{Li}_{1.15}\text{Na}_{0.05}\text{Ni}_{0.2}\text{Mn}_{0.6}\text{O}_2$. The synthetic process was as follows: (1) the co-precipitated hydroxides of Ni and Mn were synthesized by adding dissolved transition metal acetates into a 0.1-M NaOH solution drop by drop, and then the hydroxides were dried at 120 °C for 12 h to get the final coprecipitation precursor $\text{Ni}_{0.5}\text{Mn}_{1.5}(\text{OH})_4$; (2) stoichiometric amounts of $\text{C}_2\text{H}_3\text{O}_2\text{Li}\cdot 2\text{H}_2\text{O}$ (LiAC) (5% excess), $\text{CH}_3\text{COONa}\cdot 3\text{H}_2\text{O}$ (NaAC) or Na_2CO_3 , and $\text{Ni}_{0.5}\text{Mn}_{1.5}(\text{OH})_4$ were dispersed into alcohol to form a homogeneous slurry; (3) the above homogeneous mixture was milled for 8 h, with a revolving of 200 rpm; (4) the obtained slurry was dried at 120 °C for 24 h; and (5) the obtained powder was decomposed at 450 °C for 5 h, and then the particles were annealed at 850 °C for 8 h in air to form the final $\text{Li}_{1.2}\text{Ni}_{0.2}\text{Mn}_{0.6}\text{O}_2$ and $\text{Li}_{1.15}\text{Na}_{0.05}\text{Ni}_{0.2}\text{Mn}_{0.6}\text{O}_2$ cathode materials. For the convenience of representation, $\text{Li}_{1.2}\text{Ni}_{0.2}\text{Mn}_{0.6}\text{O}_2$ was indicated as “a,” $\text{Li}_{1.15}\text{Na}_{0.05}\text{Ni}_{0.2}\text{Mn}_{0.6}\text{O}_2$ prepared using LiAC and NaAC as raw materials was indicated as “b,” and $\text{Li}_{1.15}\text{Na}_{0.05}\text{Ni}_{0.2}\text{Mn}_{0.6}\text{O}_2$ using LiAC and Na_2CO_3 as raw materials was indicated as “c,” respectively.

Characterization of materials

The structure of as-prepared materials were measured by powder X-ray diffraction (XRD, D/MAX2500PC) using a Cu K α radiation source in the two-theta range of 10 to 90°. The morphology of the powders was collected on a field-emission scanning electron microscope (SEM, JEOL, JSM-7001F). Transmission electron microscope (TEM, Hitachi-7650) and energy dispersive spectroscopy (EDS) were also used for further analysis.

For preparing a positive electrode film, 80 wt% of prepared powders were mixed with 10 wt% of acetylene black and 10 wt% of binder until slurry was obtained. Then, the blended slurry was coated onto an aluminum foil. The positive and lithium foil negative electrodes of the cell for the test were separated by a porous polypropylene film, and the solvent including 1 mol L⁻¹ LiPF₆ in EC/EMC/DMC (1:1:1 in volume) was selected as the electrolyte. Assembled cells were examined between 2.0 and 4.8 V at room temperature by the NEWARE battery circler. The electrochemical impedance spectroscopy (EIS) results were tested in the frequency range of 0.01 Hz–100 kHz with a CHI660D electrochemical analyzer.

Results and discussion

Figure 1a shows XRD patterns of all cathode materials. The selected segments (18–19°) and (44–45°) of XRD patterns are shown in Fig. 1b, c. These main diffraction peaks of all patterns are assigned to the standard diffraction peaks of hexagonal a-NaFeO₂ structure (R-3m space group), which

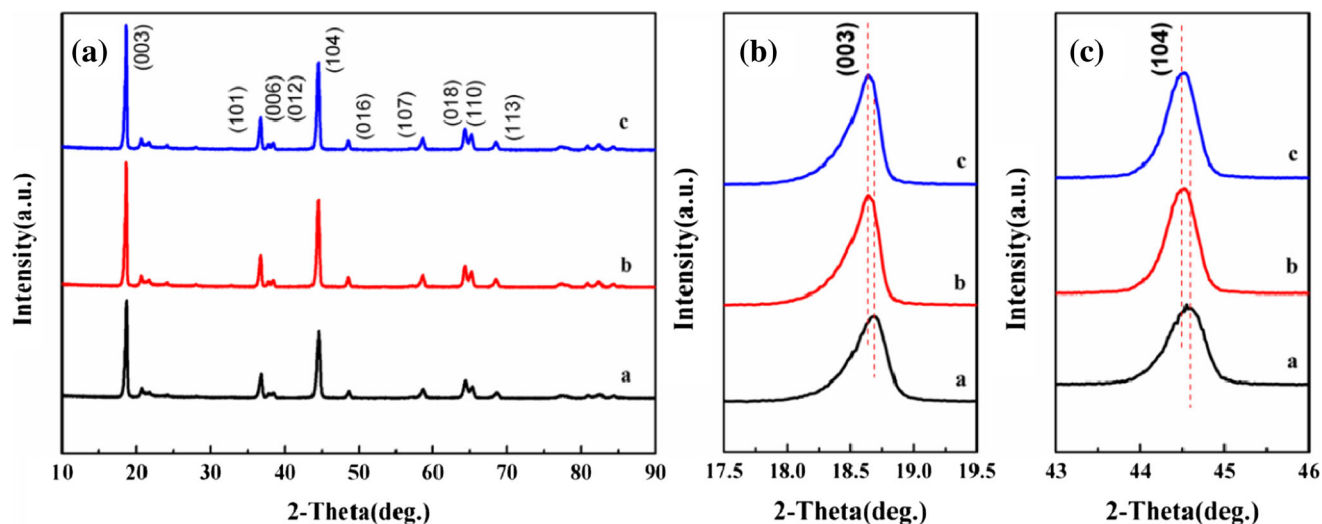


Fig. 1 XRD patterns of the as-prepared samples using different raw materials: **a** $\text{Li}_{1.2}\text{Ni}_{0.2}\text{Mn}_{0.6}\text{O}_2$ (LiAC), **b** $\text{Li}_{1.15}\text{Na}_{0.05}\text{Ni}_{0.2}\text{Mn}_{0.6}\text{O}_2$ (LiAC+NaAC), and **c** $\text{Li}_{1.15}\text{Na}_{0.05}\text{Ni}_{0.2}\text{Mn}_{0.6}\text{O}_2$ (LiAC+ Na_2CO_3)

correspond to the LiMO_2 ($M = \text{Ni}$ and Mn) phase. Besides, there are a few small additional peaks around $2\theta = 20\text{--}23^\circ$ that can be observed in all patterns, which is related to superstructure reflections of Li_2MnO_3 ($C2/m$ space group). It is obvious that both the (006)/(012) and (018)/(110) peaks are completely spilt, which indicates that a well-defined layered structure is obtained in the lattice. Furthermore, there is no obvious difference that can be seen among samples with different raw materials, which demonstrates that both the samples with sodium acetate and sodium carbonate can form a well-defined layered structure. In comparison with the patterns of pristine $\text{Li}_{1.2}\text{Ni}_{0.2}\text{Mn}_{0.6}\text{O}_2$, no other peaks can be detected in the $\text{Li}_{1.15}\text{Na}_{0.05}\text{Ni}_{0.2}\text{Mn}_{0.6}\text{O}_2$ samples, suggesting that Na ions are successfully introduced into the crystal lattice without any destruction to the layered structure. As shown in the enlarged sections, the (003) peak and (104) peak of Na-doped samples b and c shift slightly toward the lower angle. This observation implies that the Na ions are successfully doped into the bulk lattice so as to enlarge the Li slab space, which is because of the difference of ionic radii between the Na ion ($r_{\text{Na}^+} = 1.02 \text{ \AA}$) and Li ion ($r_{\text{Li}^+} = 0.76 \text{ \AA}$). The software MDI Jade 6.0 was employed to calculate the lattice parameters of all samples. From these data in Table 1, it is noted that Na-doped samples $\text{Li}_{1.15}\text{Na}_{0.05}\text{Ni}_{0.2}\text{Mn}_{0.6}\text{O}_2$ have greater volume than the pristine one. The a-axis constants, which are ascribed to the metal-metal interslab distance and the c-axis constants,

Table 1 Structural constants of all samples with different raw materials

Sample	<i>a</i> (Å)	<i>c</i> (Å)	<i>V</i> (Å ³)	<i>c/a</i>
a	2.85191	14.24213	100.49	4.9939
b	2.88695	14.24887	102.42	4.9356
c	2.87614	14.25362	102.24	4.9558

which are usually related to the Li slab space, both increase with the doping Na ions. The greater ionic radius of the Na ion (1.02 Å) compared with the Li ion (0.76 Å) is responsible for the expansion of the lattice parameters. The enlargement of lattice constants is beneficial for the diffusion of lithium ions, indicating an enhanced electrochemical performance. And all the *c/a* ratios are more than 4.9, further demonstrating that a high ordered layer structure was obtained for all samples with different raw materials.

The chemical composition of the as-prepared samples is analyzed by inductive coupled plasma mass spectrometry (ICP-MS). The element content of the three samples is listed in Table 2. According to the ICP results, all samples exhibit a similar element content to the theoretical stoichiometry. Compared with sample-a, the Li content is decreasing from 1.187 to 1.141 of sample-b and 1.143 of sample-c with the Na-doping process. Meanwhile, the molar number of Na of sample-b and sample-c is determined as 0.052 and 0.047, respectively. It is in good agreement with the amount of NaAC in the doping process. Generally, NaAC is selected as the better Na source to synthesize the Na-doping samples because of its low decomposition temperature. Therefore, the analyzed element content of sample-b is in better accordance with the theoretical stoichiometry.

Figure 2a–c shows the SEM images of the $\text{Li}_{1.2}\text{Ni}_{0.2}\text{Mn}_{0.6}\text{O}_2$ and $\text{Li}_{1.15}\text{Na}_{0.05}\text{Ni}_{0.2}\text{Mn}_{0.6}\text{O}_2$ composites. All materials present

Table 2 The ICP-MS elemental analysis results of $\text{Li}_{1.2}\text{Ni}_{0.2}\text{Mn}_{0.6}\text{O}_2$ and $\text{Li}_{1.15}\text{Na}_{0.05}\text{Ni}_{0.2}\text{Mn}_{0.6}\text{O}_2$ materials

Sample	Target stoichiometry	Li	Ni	Mn	O	Na
a	$\text{Li}_{1.2}\text{Ni}_{0.2}\text{Mn}_{0.6}\text{O}_2$	1.187	0.207	0.620	2	0
b	$\text{Li}_{1.15}\text{Na}_{0.05}\text{Ni}_{0.2}\text{Mn}_{0.6}\text{O}_2$	1.143	0.201	0.614	2	0.052
c	$\text{Li}_{1.15}\text{Na}_{0.05}\text{Ni}_{0.2}\text{Mn}_{0.6}\text{O}_2$	1.141	0.216	0.610	2	0.047

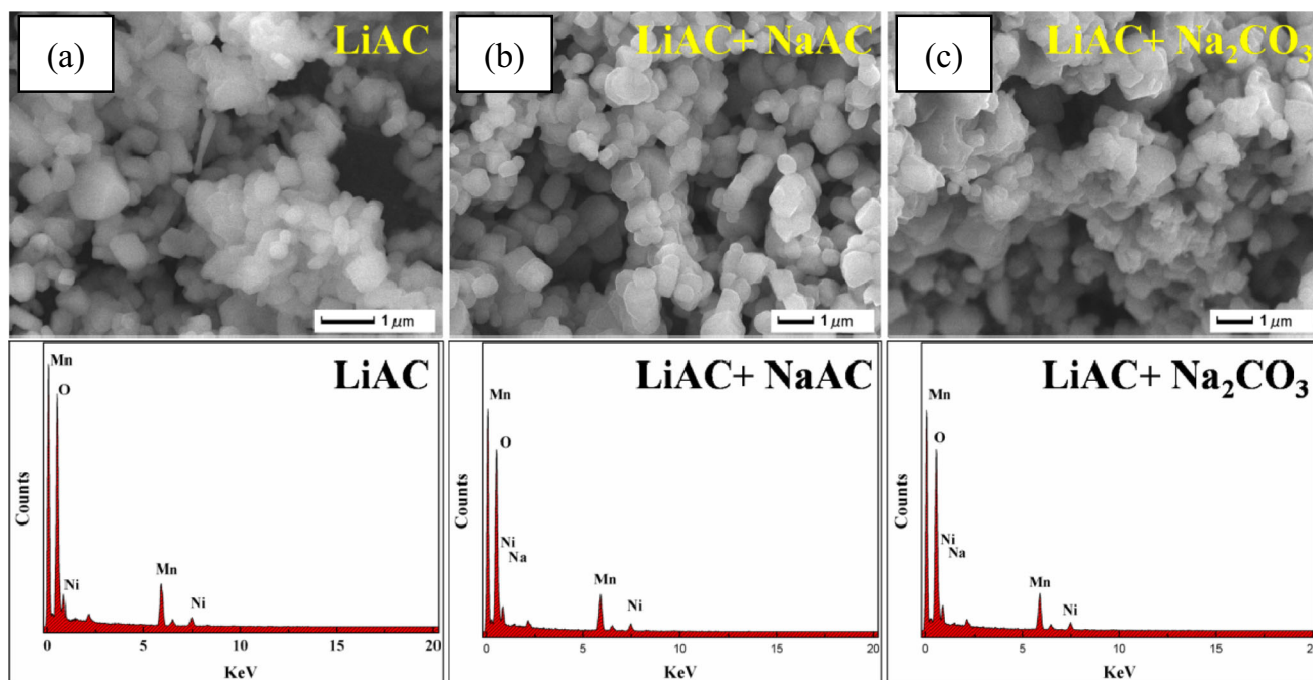


Fig. 2 SEM images and EDS spectra of **a** sample $\text{Li}_{1.2}\text{Ni}_{0.2}\text{Mn}_{0.6}\text{O}_2$ (LiAC), **b** sample $\text{Li}_{1.15}\text{Na}_{0.05}\text{Ni}_{0.2}\text{Mn}_{0.6}\text{O}_2$ (LiAC+NaAC), and **c** sample $\text{Li}_{1.15}\text{Na}_{0.05}\text{Ni}_{0.2}\text{Mn}_{0.6}\text{O}_2$ (LiAC+ Na_2CO_3)

almost the same particle sizes of about 300–800 nm, which is because of their same manufacturing process and same precursor $\text{Ni}_{0.5}\text{Mn}_{1.5}(\text{OH})_4$. However, image (c) clearly indicated that a severe agglomeration of particles occurred in the sample using Na_2CO_3 as raw material. In addition, with the increase of the sodium content, there is no obvious difference existing between the a- $\text{Li}_{1.2}\text{Ni}_{0.2}\text{Mn}_{0.6}\text{O}_2$ and b- $\text{Li}_{1.15}\text{Na}_{0.05}\text{Ni}_{0.2}\text{Mn}_{0.6}\text{O}_2$ particles. Thus, it can be confirmed from the SEM images that the formation of the composites using LiAC and NaAC as Li source and Na source is more successful, indicating that different raw materials can have a large effect on the morphology on the particles. As a further quantitative analysis of the pristine sample and the Na-doped samples b and c, these particles were examined via EDS. The results in Fig. 2 and Table 3 show that about 5 at% Na can be detected on the surface of the particles of Na-doped samples, and the transition metal atom relative ratios have no evident difference between these two samples, which is in accordance with the theoretical ratios ($\text{Mn}/\text{Ni} = 6:2$). In addition, Brunauer–Emmett–Teller (BET) analysis is utilized to investigate the specific surface area of different samples, as illustrated

Table 3 EDS analysis of element amount of Mn/Ni/Na of sample-a $\text{Li}_{1.2}\text{Ni}_{0.2}\text{Mn}_{0.6}\text{O}_2$ (LiAC), sample-b $\text{Li}_{1.15}\text{Na}_{0.05}\text{Ni}_{0.2}\text{Mn}_{0.6}\text{O}_2$ (LiAC+NaAC), and sample-c $\text{Li}_{1.15}\text{Na}_{0.05}\text{Ni}_{0.2}\text{Mn}_{0.6}\text{O}_2$ (LiAC+ Na_2CO_3)

Sample	O	Mn	Ni	Na	Mn/Ni/Na
a	78.48	15.33	5.43	–	0.600/0.213/0
b	79.21	14.83	5.23	1.25	0.600/0.212/0.051
c	79.14	14.95	5.41	1.33	0.600/0.217/0.053

in Table 4. It is clear that the three samples have a similar specific surface area of $12\text{--}13\text{ m}^2\text{ g}^{-1}$ which can supply sufficient reaction sites and is beneficial for electrolyte access. Meanwhile, there are no significant differences of surface area between bare sample and Na-doped samples. Therefore, the primary reason for improved electrochemical performance caused by Na-doping can not only be attributed to the microscopic properties such as morphology and particle size.

HR-TEM images of pristine $\text{Li}_{1.2}\text{Ni}_{0.2}\text{Mn}_{0.6}\text{O}_2$ and $\text{Li}_{1.15}\text{Na}_{0.05}\text{Ni}_{0.2}\text{Mn}_{0.6}\text{O}_2$ particles with different raw materials are shown in Fig. 3. From the detailed morphologies, it can be seen that all the synthesized materials retain well the layered structure. In addition, clear lattice fringes can be measured from the corresponding FFT patterns of these high-resolution TEM images; these fringes with d-spacing of 0.47 nm are well matched to the interplanar distance of the (003) plane of the LiMO_2 ($M = \text{Ni}, \text{Co}$ or Mn) layered structure inferred from XRD patterns. These inserted FFT images that correspond to the selected area also prove that a single-crystalline structure with high crystallinity has been formed in the individual particles. This observation is in good accordance with XRD results [34].

As illustrated in Fig. 4, X-ray photoelectron spectrum (XPS) is utilized to investigate the valence state of transition

Table 4 The BET surface area analysis for all samples

Sample	Surface area ($\text{m}^2\text{ g}^{-1}$)
a	12.625
b	12.147
c	12.355

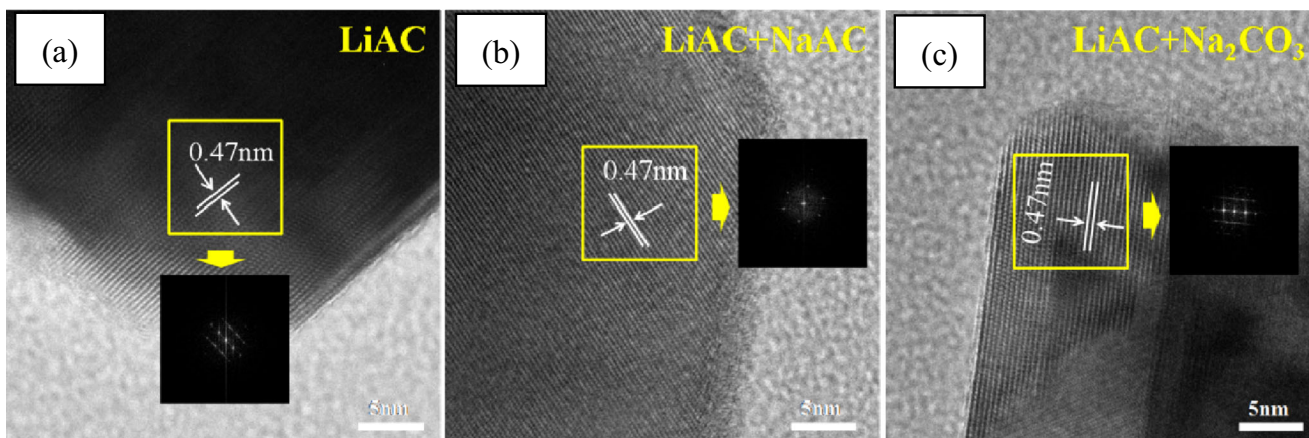


Fig. 3 TEM images of **a** sample a $\text{Li}_{1.2}\text{Ni}_{0.2}\text{Mn}_{0.6}\text{O}_2$ (LiAC), **b** sample b $\text{Li}_{1.15}\text{Na}_{0.05}\text{Ni}_{0.2}\text{Mn}_{0.6}\text{O}_2$ (LiAC+NaAC), and **c** sample c $\text{Li}_{1.15}\text{Na}_{0.05}\text{Ni}_{0.2}\text{Mn}_{0.6}\text{O}_2$ (LiAC+ Na_2CO_3) with corresponding indexed FFT patterns

metal elements in the surface of the as-prepared materials. It is clear that for all the samples, the binding energies (BEs) of $\text{Ni}_{2p_{3/2}}$ (Fig. 4b) and $\text{Mn}_{2p_{3/2}}$ (Fig. 4c) are located at 854.7 and 642.4 eV, respectively, which is close to the values of Ni^{2+} and Mn^{4+} in layered oxides $\text{Li}[\text{Li}_{1/3-2x/3}\text{Ni}_x\text{Mn}_{2/3-x/3}]\text{O}_2$. Furthermore, as shown in Fig. 4d, the peak of Na 1s can be observed in sample-b and sample-c. The peak position is located at a binding energy of approximately 1072.89 eV, which

is in good agreement with the standard binding energy of Na^+ oxide, suggesting that the Na element appear as Na^+ in the Na-doped samples. All the XPS data further indicate that the Na element has been successfully introduced into the bulk phase as Na^+ , and the introduction of Na^+ has no influence on the oxidation state of the transition metal ion.

The initial charge and discharge profiles at 0.1 C are plotted in Fig. 5. The corresponding initial charging/discharging data

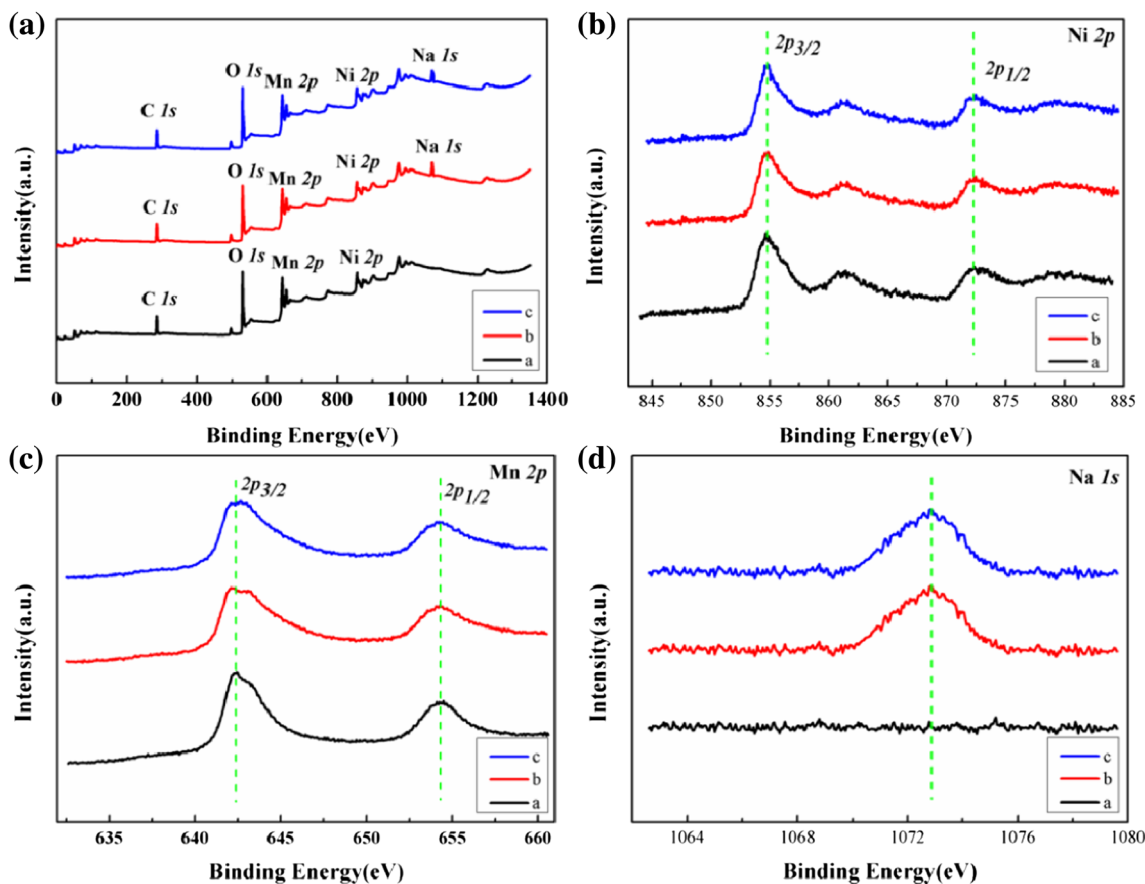


Fig. 4 XPS spectra for all samples in the region of **a** survey spectrum, **b** Ni 2p, **c** Mn 2p, and **d** Na 1s

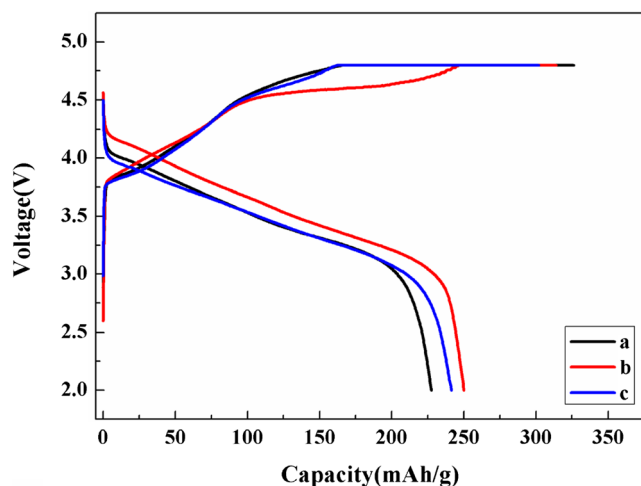


Fig. 5 Initial charge/discharge curves of sample-a $\text{Li}_{1.2}\text{Ni}_{0.2}\text{Mn}_{0.6}\text{O}_2(\text{LiAC})$, sample-b $\text{Li}_{1.15}\text{Na}_{0.05}\text{Ni}_{0.2}\text{Mn}_{0.6}\text{O}_2(\text{LiAC}+\text{NaAC})$, and sample-c $\text{Li}_{1.15}\text{Na}_{0.05}\text{Ni}_{0.2}\text{Mn}_{0.6}\text{O}_2(\text{LiAC}+\text{Na}_2\text{CO}_3)$

were summarized in Table 5. The pristine sample LNMO delivers a similar high initial charge/discharge capacity of $326/227 \text{ mAh g}^{-1}$. The pristine electrode displays an initial coulombic efficiency of about 70%. With the increasing amount of Na, the discharge capacity at 0.1 C increases to 249 mAh g^{-1} for the b sample, 241 mAh g^{-1} for the c sample, respectively. The initial charge profiles of all samples similarly present a slope below 4.5 V and another high potential plateau at 4.5 V. During the first charge process, the first voltage ramp is related to the reversible extraction of Li^+ from the Li-layers and the second long potential plateau can be attributed to the Li_2O extraction from Li_2MnO_3 components. Generally, the initial charge/discharge capacities for the b and c samples are better than the bare sample. The reason for the better initial performance of Na-doped samples can be explained in two aspects. One can be attributed to the highly ordered and stable structure caused by the Na-doping process. The unchangeable doped Na ions with larger ionic radius can suppress collapse of the lattice structure, resulting in a mitigation of irreversible removal of Li_2O in the first cycle. The other one is that the incorporation of Na leads to a further activation of the reduction of the manganese component. Furthermore, there is no obvious enlargement of the reversible capacity between the samples from different raw materials. Based on the mechanism mentioned above, the Na-doping process has a positive influence on the coulombic

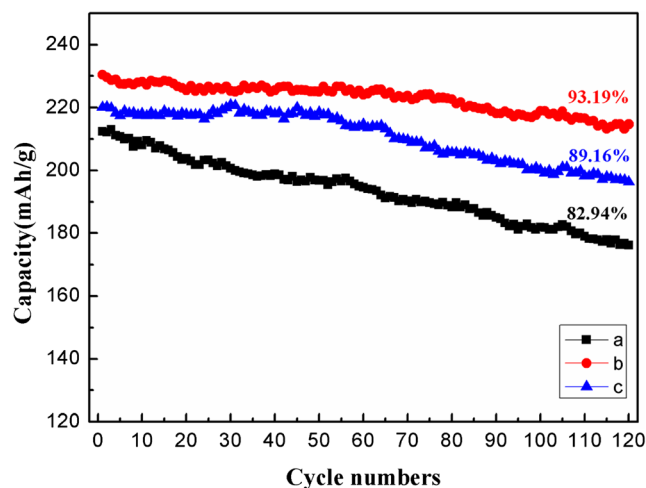


Fig. 6 Cycling performance of sample-a $\text{Li}_{1.2}\text{Ni}_{0.2}\text{Mn}_{0.6}\text{O}_2(\text{LiAC})$, sample-b $\text{Li}_{1.15}\text{Na}_{0.05}\text{Ni}_{0.2}\text{Mn}_{0.6}\text{O}_2(\text{LiAC}+\text{NaAC})$, and sample-c $\text{Li}_{1.15}\text{Na}_{0.05}\text{Ni}_{0.2}\text{Mn}_{0.6}\text{O}_2(\text{LiAC}+\text{Na}_2\text{CO}_3)$

efficiency of the cathode materials. However, there is no obvious improvement between the different raw materials.

To evaluate the effects of different raw materials on the cycling stability, all the cathode materials were measured in the voltage range of 2.0 to 4.8 V at 25 °C. An activation process was carried out at 0.1C for seven cycles before all the samples were tested at 0.2 C. As presented in Fig. 6, Na-doped electrodes show the higher discharge capacities than the pristine sample. Among these samples, the b electrode ($\text{LiAC}+\text{NaAC}$) delivers a best cycling capacity of 230 and 215 mAh g^{-1} at the first and 120th cycles, respectively. Its retention ratio is about 93.19%. Oppositely, the pristine sample-a (LiAC) exhibits a lower discharge capacity of 176 mAh g^{-1} after 120 cycles with a capacity retention ratio of 82.94%. Further, the discharge capacity of sample-c ($\text{LiAC}+\text{Na}_2\text{CO}_3$) at first and 120th cycles is 220 and 196 mAh g^{-1} , respectively. The capacity retention of sample-c is as high as 89.16% up from 82.94% for the pristine sample. The improved electrochemical performance of the Na-doped electrodes is mainly attributed to the doped Na ions in the Li sites can steady available the lattice structure to inhibit the phase transformation during the lithium insertion and extraction. And the superior cycling performance of sample-b which is apparently better than sample-c is due to the better structure has been formed, as proved in XRD and SEM results. The lithium acetate ($\text{C}_2\text{H}_3\text{O}_2\text{Li}$) and sodium

Table 5 First charge/discharge capacity and coulomb efficiency of synthesized samples

Samples	Charge capacity ($\text{mAh}\cdot\text{g}^{-1}$)	Discharge capacity ($\text{mAh}\cdot\text{g}^{-1}$)	Irreversible capacity loss ($\text{mAh}\cdot\text{g}^{-1}$)	Coulomb efficiency (%)
a	326	227	99	69.63
b	313	249	64	79.55
c	301	241	60	79.73

acetate (CH_3COONa) were evidenced as better Li and Na source.

Voltage decay upon cycling, which mainly attributed to the layer-spinel structure conversion, is a main obstruction for the application of layered lithium-rich materials. Figure 7 demonstrates the discharge mean voltage plots of all the samples during 50 cycles. Note that the discharge voltage of sample-a acutely decreases from 3.42 to 2.95 V after 50 cycles ($\Delta E = 0.47$ V). As for the Na-doped samples, both sample-b and sample-c display a lower discharge voltage reduction of 0.34 and 0.39 V upon 50 cycles, corresponding to a low voltage reduction of 0.0068 and 0.0078 V at one cycle, respectively. As expected, the voltage fading rate of Na-doped samples efficiently are lower than the pristine sample, which is due to the suppression of cation mixing. In addition, the better stable operating voltage for electrodes using sodium acetate as raw materials is mainly attributed to their better structural stability which is easier to form in the lower melting point. Figure 7b–d shows the discharge curves of different samples at first, 20th, 40th, 60th, and 80th cycles, it is clear that the cycle stability of sample-b and sample-c are better than sample-a.

Figure 8 displays the rate capability of different electrodes. These as-prepared samples were discharged at different current densities (0.1, 0.2, 0.5, 1.0, 2.0, 5.0, and 0.1 C) after

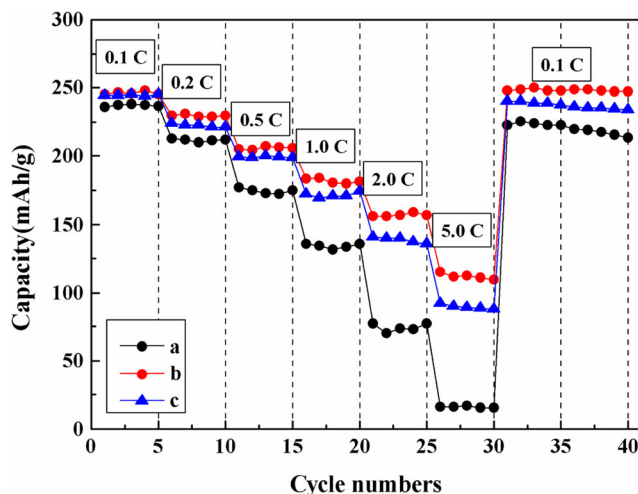


Fig. 8 Rate performance of sample-a $\text{Li}_{1.2}\text{Ni}_{0.2}\text{Mn}_{0.6}\text{O}_2$ (LiAC), sample-b $\text{Li}_{1.15}\text{Na}_{0.05}\text{Ni}_{0.2}\text{Mn}_{0.6}\text{O}_2$ (LiAC + NaAC), and sample-c $\text{Li}_{1.15}\text{Na}_{0.05}\text{Ni}_{0.2}\text{Mn}_{0.6}\text{O}_2$ (LiAC + Na_2CO_3)

charging at a constant current density (0.1 C). Obviously, the discharge capacities of Na-doped samples at different current densities are higher than those of the pristine sample, especially at comparatively high densities. Specifically, sample-b exhibits the highest discharge capacities of 246, 230, 206, 179,

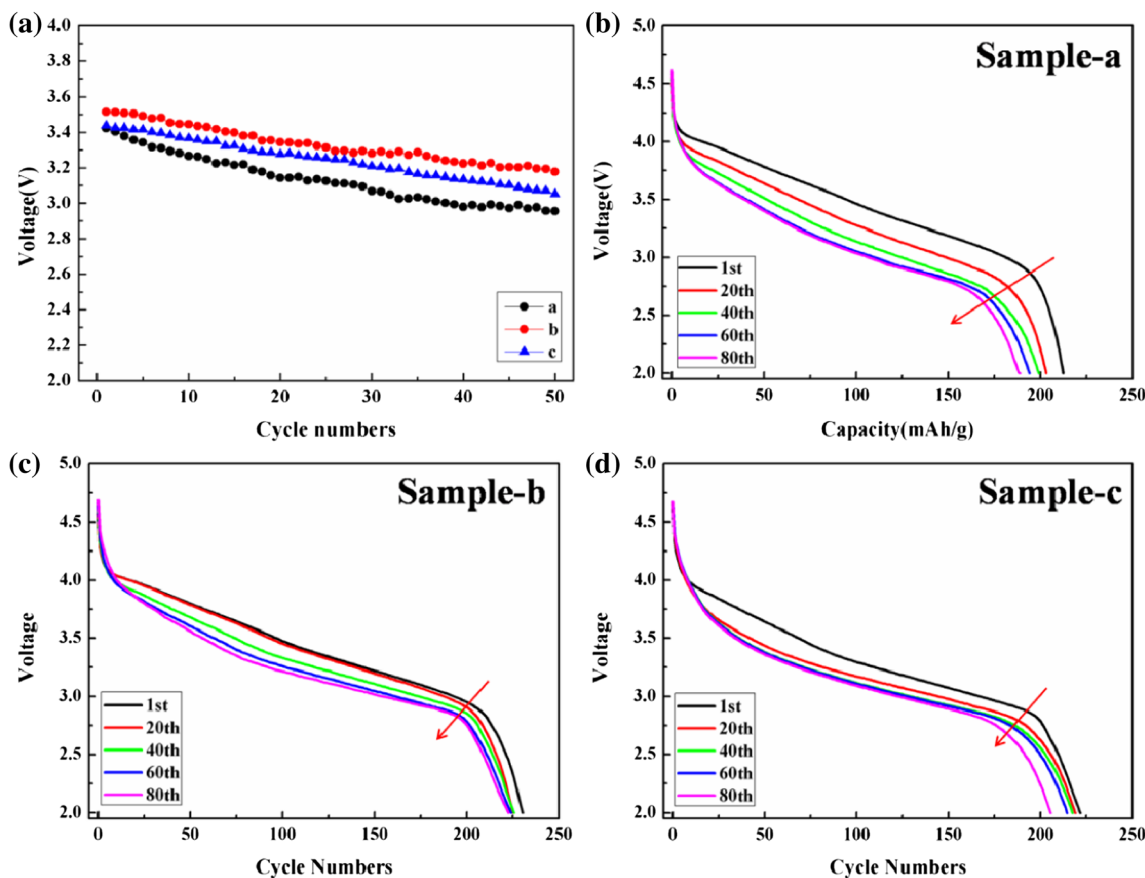


Fig. 7 a Mean voltage and discharge profiles at different cycles of b sample a $\text{Li}_{1.2}\text{Ni}_{0.2}\text{Mn}_{0.6}\text{O}_2$ (LiAC), c sample b $\text{Li}_{1.15}\text{Na}_{0.05}\text{Ni}_{0.2}\text{Mn}_{0.6}\text{O}_2$ (LiAC+NaAC), and d sample c $\text{Li}_{1.15}\text{Na}_{0.05}\text{Ni}_{0.2}\text{Mn}_{0.6}\text{O}_2$ (LiAC+ Na_2CO_3)

155, and 109 mAh g⁻¹ at 0.1, 0.2, 0.5, 1.0, 2.0, and 5.0 C, respectively, compared with 235, 210, 175, 133, 69, and 15 mAh g⁻¹ for the pristine sample-a. The reason for the improvement of the rate capability is that the expanded Li space due to the Na-doping process can decrease the resistance for Li diffusion and accelerate the electron migration. In addition, these cells were also tested at 0.1 C after cycled at high current densities. As seen in Fig. 8, the capacity at 0.1 C of sample-b after cycled at high current densities is apparently higher than sample-a and sample-c even better than its initial capacity at 0.1 C, which demonstrates that sample-b maintains a good cycle stability after cycled at high current densities.

The structural stability of the materials was evidenced by the XRD experiment. XRD patterns of the Li_{1.2}Ni_{0.2}Mn_{0.6}O₂ and Li_{1.15}Na_{0.05}Ni_{0.2}Mn_{0.6}O₂ electrodes cycled after 100 cycles are shown in Fig. 9. It is clearly observed that all the three samples show broader peaks and lower intensity after 100 cycles. However, the XRD patterns of sample-b is closer to the XRD patterns of its pristine electrode before cycling, suggesting that the sample-b electrode has a strong structural stability during cycling. Besides, both the (003) peak and (104) peak move slightly toward the lower angle region after 100 cycles. As seen in the detailed patterns, the (003) peak and the (104) peak of sample-b and sample-c display a lower change than sample-a. This phenomenon also suggests that a stronger structural stability has been achieved for the Na-doped electrodes, which contributes to the excellent cycling performance for the Na-doped samples during the long-term cycling.

EIS provides information about the kinetics of electrochemical reactions of electrodes. [35] To better understand the effects of raw materials on electrochemical performance, all the samples are examined by EIS tests. The measurements were carried out in the charged state of 5 V after 1 cycle tested at 0.1 C with three electrodes system. The measured

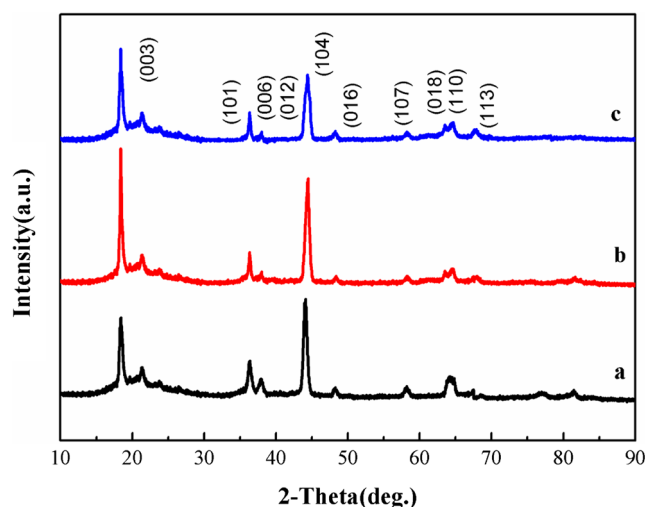


Fig. 9 XRD patterns of sample-a Li_{1.2}Ni_{0.2}Mn_{0.6}O₂ (LiAC), sample-b Li_{1.15}Na_{0.05}Ni_{0.2}Mn_{0.6}O₂ (LiAC + NaAC), and sample-c Li_{1.15}Na_{0.05}Ni_{0.2}Mn_{0.6}O₂ (LiAC + Na₂CO₃)

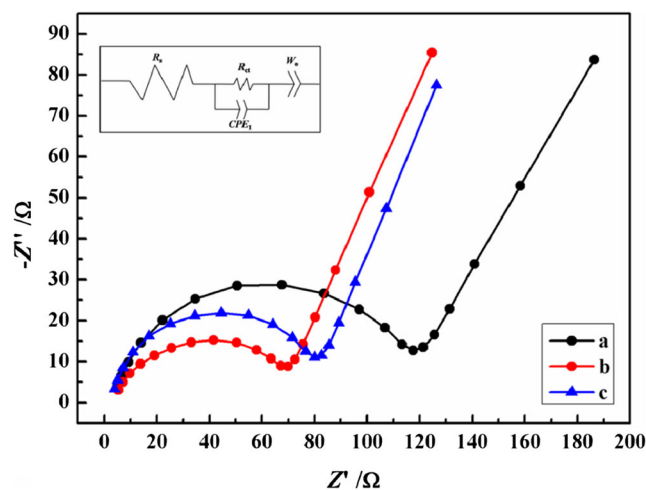


Fig. 10 Nyquist plots for the samples using different raw materials after the first cycle: sample-a Li_{1.2}Ni_{0.2}Mn_{0.6}O₂ (LiAC), sample-b Li_{1.15}Na_{0.05}Ni_{0.2}Mn_{0.6}O₂ (LiAC + NaAC), and sample-c Li_{1.15}Na_{0.05}Ni_{0.2}Mn_{0.6}O₂ (LiAC + Na₂CO₃) and equivalent circuit

impedance spectra are presented in Fig. 10. A high-frequency semicircle and a low-frequency tail are observed. Generally, an intercept at the Z real-axis in the high-frequency region corresponded to ohm resistance (R_s). The high-frequency semicircle is related to charge transfer resistance (R_{ct}). The low-frequency tail is associated with the Li ion diffusion process in the solid phase of the electrode. Each impedance spectrum is fitted with suggested equivalent circuit model to give simulation of the ohm resistance (R_s) and charge transfer resistance (R_{ct}). As seen in Table 6, a rapid decrease of the surface charge transfer resistance and ohm resistance has been observed in sample-b. The sample-b cathode shows the lowest charge transfer resistance (R_{ct}). Furthermore, based on the Warburg diffusion supported by the low-frequency region, the diffusion coefficient (D_{Li^+}) of lithium ions is calculated based on the following equations:

$$D = 0.5 [RT/An^2 F^2 \sigma_w C_0]^2 \quad (1)$$

$$Z' = R_s + R_{ct} + \sigma_w \omega^{-0.5} \quad (2)$$

As shown in Eq. (1), R is the ideal gas constant, T is the absolute temperature, n is the number of electrons per

Table 6 Electrolyte resistance (R_s), charge transfer resistance (R_{ct}), and diffusion coefficient (D_{Li^+}) of sample-a Li_{1.2}Ni_{0.2}Mn_{0.6}O₂ (LiAC), sample-b Li_{1.15}Na_{0.05}Ni_{0.2}Mn_{0.6}O₂ (LiAC + NaAC), and sample-c Li_{1.15}Na_{0.05}Ni_{0.2}Mn_{0.6}O₂ (LiAC + Na₂CO₃)

	a	b	c
$R_s(\Omega)$	4.486	1.645	2.241
$R_{ct}(\Omega)$	209.9	127.6	188.4
$D_{Li}(\text{cm}^2 \text{s}^{-1})$	6.15×10^{-14}	2.24×10^{-13}	9.95×10^{-14}

molecule during the charge/discharge process, F is the Faraday constant, C_0 is the concentration of Li^+ in pre unit cell, A is surface area of the electrode in cm^2 , and σ is the Warburg factor which has relationship with Z' (shown in Eq. (2)). On the basis of the above information, the lithium-ion diffusion coefficients of the pristine $\text{Li}_{1.2}\text{Ni}_{0.2}\text{Mn}_{0.6}\text{O}_2$ and $\text{Li}_{1.15}\text{Na}_{0.05}\text{Ni}_{0.2}\text{Mn}_{0.6}\text{O}_2$ cathodes after 1 cycle are calculated. As shown in Table 4, the lithium diffusion coefficients of Na-doped sample-b ($2.24 \times 10^{-13} \text{ cm}^2 \text{ s}^{-1}$) and sample-c ($9.95 \times 10^{-14} \text{ cm}^2 \text{ s}^{-1}$) are better than sample-a ($6.15 \times 10^{-14} \text{ cm}^2 \text{ s}^{-1}$). These results revealed that the Na-doping process and selecting sodium acetate as raw materials has good influence on the improvement of the lithium diffusion coefficient of electrodes, further proof that the appropriate raw materials have a positive effect on the electrochemical performance.

Conclusion

The effect of raw materials on the structure, morphology, and electrochemical performance of Li-rich $\text{Li}_{1.2}\text{Ni}_{0.2}\text{Mn}_{0.6}\text{O}_2$ cathode materials has been systematically investigated. The results demonstrate that the electrochemical performance of Na-doped cathodes is sensitive to the raw materials. The best-performing cathode $\text{Li}_{1.15}\text{Na}_{0.05}\text{Ni}_{0.2}\text{Mn}_{0.6}\text{O}_2$ material was achieved with LiAC and NaAC as raw materials; it is capable of retaining 96% of its initial capacity after 80 cycles at 0.2 C (retaining 93% of its initial capacity after 120 cycles at 0.2 C) and delivering a capacity above 109 mAh g^{-1} at 5 C rate. Sodium carbonate leads to worse cycling stability and rate capability because of its higher melting point that is closely related to the structure. The findings highlight the importance of optimizing the raw materials for preparing the Na-doped Li-rich Mn-based cathode materials. Lithium acetate and sodium acetate have been considered as the best Li source and Na source.

Acknowledgments This study was financially supported by the National Natural Science Foundation of China (Nos. 51504225 and 51404220) and Natural Science Foundation of Jiangsu Province (BK20150506 and BK20150535).

References

- Armand M, Tarascon JM (2008) Building better batteries. *Nature* 451(7179):652–657
- Etacheri V, Marom R, Ran E (2011) Challenges in the development of advanced Li-ion batteries: a review. *Energy Environ Sci* 4(9):3243–3262
- Nitta N, Wu F, Lee JT (2015) Li-ion battery materials: present and future. *Mater Today* 18(5):252–264
- Whittingham MS (2004) Lithium batteries and cathode materials. *Cheminform* 35(50):4271–4301
- Wei HH, Zhang Q, Xu QJ (2018) Baby diaper-inspired construction of 3D porous composites for long-term lithium-ion batteries. *Adv Funct Mater* 28(3):1704440
- Wang X, Xu QJ, Min YL (2018) Self-evaporating from inside to outside to construct cobalt oxide nanoparticles-embedded nitrogen-doped porous carbon nanofibers for high-performance lithium ion batteries. *Chem Eng J* 334:1642–1649
- Wang J, He X, Paillard E (2016) Lithium- and manganese-rich oxide cathode materials for high-energy lithium ion batteries. *Adv Energy Mater* 6(21)
- Liu YJ, Gao YY, Lv J (2013) A facile method to synthesize carbon coated $\text{Li}_{1.2}\text{Ni}_{0.2}\text{Mn}_{0.6}\text{O}_2$, with improved performance. *Mater Res Bull* 48(11):4930–4934
- Chong S, Wu Y, Chen Y (2017) A strategy of constructing spherical core-shell structure of $\text{Li}_{1.2}\text{Ni}_{0.2}\text{Mn}_{0.6}\text{O}_2@ \text{Li}_{1.2}\text{Ni}_{0.2}\text{Mn}_{0.4}\text{O}_2$, cathode material for high-performance lithium-ion batteries. *J Power Source* 356:153–162
- Lee DK, Park SH, Amine K (2006) High capacity $\text{Li}[\text{Li}_{0.2}\text{Ni}_{0.2}\text{Mn}_{0.6}]\text{O}_2$ cathode materials via a carbonate coprecipitation method. *J Power Sources* 162(2):1346–1350
- Li L, Wang L, Zhang X (2016) 3D reticular $\text{Li}_{1.2}\text{Ni}_{0.2}\text{Mn}_{0.6}\text{O}_2$ cathode material for lithium-ion batteries. *ACS Appl Mater Interfaces* 9(2)
- Zhang L, Wu B, Li N (2013) Rod-like hierarchical nano/micro $\text{Li}_{1.2}\text{Ni}_{0.2}\text{Mn}_{0.6}\text{O}_2$ as high performance cathode materials for lithium-ion batteries. *J Power Sources* 240(1):644–652
- He W, Yuan D, Qian J (2013) Enhanced high-rate capability and cycling stability of Na-stabilized layered $\text{Li}_{1.2}[\text{Co}_{0.13}\text{Ni}_{0.13}\text{Mn}_{0.54}]\text{O}_2$ cathode material. *J Mater Chem A* 1(37):11397–11403
- Guo H, Xia Y (2017) Stabilization effects of Al doping for enhanced cycling performances of Li-rich layered oxides. *Ceram Int* 43:13845–13852
- Feng X, Gao Y, Ben L (2016) Enhanced electrochemical performance of Ti-doped $\text{Li}_{1.2}\text{Mn}_{0.54}\text{Co}_{0.13}\text{Ni}_{0.13}\text{O}_2$ for lithium-ion batteries. *J Power Sources* 317:74–80
- Song B, Zhou C (2014) Advances in sustain stable voltage of Cr-doped Li-rich layered cathodes for lithium-ion batteries. *J Electrochem Soc* 161:A1723–A1730
- Chen H, Hu Q, Huang Z (2016) Synthesis and electrochemical study of Zr-doped $\text{Li}[\text{Li}_{0.2}\text{Mn}_{0.54}\text{Ni}_{0.13}\text{Co}_{0.13}]\text{O}_2$, as cathode material for Li-ion battery. *Ceram Int* 42:263–269
- Liu X, Huang T, Yu A (2014) Fe doped $\text{Li}_{1.2}\text{Mn}_{0.6-x}\text{Ni}_{0.2-x}\text{Fe}_x\text{O}_2$ ($x \leq 0.1$) as cathode materials for lithium-ion batteries. *Electrochim Acta* 133:555–563
- Liu YJ, Zhang ZQ, Fu Y (2016) Investigation the electrochemical performance of $\text{Li}_{1.2}\text{Ni}_{0.2}\text{Mn}_{0.6}\text{O}_2$ cathode material with ZnAl_2O_4 coating for lithium ion batteries. *J Alloys Compd* 685:523–532
- Wang Z, Liu E (2013) Cycle performance improvement of Li-rich layered cathode material $\text{Li}[\text{Li}_{0.2}\text{Mn}_{0.54}\text{Ni}_{0.13}\text{Co}_{0.13}]\text{O}_2$ by ZrO_2 coating. *Surf Coat Technol* 235:570–576
- Zou G, Yang X, Wang X (2014) Improvement of electrochemical performance for Li-rich spherical $\text{Li}_{1.3}[\text{Ni}_{0.35}\text{Mn}_{0.65}]\text{O}_{2+x}$ modified by Al_2O_3 . *J Solid State Electrochem* 18:1789–1797
- Zheng J, Li J, Zhang ZR (2008) The effects of TiO_2 coating on the electrochemical performance of $\text{Li}[\text{Li}_{0.2}\text{Mn}_{0.54}\text{Ni}_{0.13}\text{Co}_{0.13}]\text{O}_2$ cathode material for lithium-ion battery. *Solid State Ionics* 179:1794–1799
- Wu F, Zhang X (2015) Multifunctional AlPO_4 coating for improving electrochemical properties of low-cost $\text{Li}[\text{Li}_{0.2}\text{Fe}_{0.1}\text{Ni}_{0.15}\text{Mn}_{0.55}]\text{O}_2$ cathode materials for lithium-ion batteries. *ACS Appl Mater Interfaces* 7:3773–3781
- Lee SH, Koo BK (2008) Effect of $\text{Co}_3(\text{PO}_4)_2$ coating on $\text{Li}[\text{Co}_{0.1}\text{Ni}_{0.15}\text{Li}_{0.2}\text{Mn}_{0.55}]\text{O}_2$ cathode material for lithium rechargeable batteries. *J Power Sources* 184:276–283

25. Pang S, Wang Y (2016) The effect of AlF_3 modification on the physicochemical and electrochemical properties of Li-rich layered oxide. *Ceram Int* 42:5397–5402
26. Jin X, Xu Q, Liu H (2014) Excellent rate capability of Mg doped $\text{Li}[\text{Li}_{0.2}\text{Ni}_{0.13}\text{Co}_{0.13}\text{Mn}_{0.54}]\text{O}_2$ cathode material for lithium-ion battery. *Electrochim Acta* 136(8):19–26
27. Liu Y, Liu D, Zhang Z, Zheng S (2017) Investigation of the structural and electrochemical performance of $\text{Li}_{1.2}\text{Ni}_{0.2}\text{Mn}_{0.6}\text{O}_2$ with Cr doping. *Ionics* (8):1–9
28. Li X, Xin HX, Liu Y (2015) Effect of niobium doping on the microstructure and electrochemical properties of lithium-rich layered $\text{Li}[\text{Li}_{0.2}\text{Ni}_{0.2}\text{Mn}_{0.6}]\text{O}_2$ as cathode materials for lithium ion batteries. *RSC Adv* 5(56):45351–45358
29. Lübke M, Shin J, Marchand P (2015) Highly pseudocapacitive Nb-doped TiO_2 high power anodes for lithium-ion batteries. *J Mater Chem A* 3(45):22908–22914
30. Xie H, Du K, Hu G (2016) The role of sodium in $\text{LiNi}_{0.8}\text{Co}_{0.15}\text{Al}_{0.05}\text{O}_2$ cathode material and its electrochemical behaviors. *J Phys Chem C* 120(6)
31. Yang Z, Guo X, Xiang W (2017) K-doped layered $\text{LiNi}_{0.5}\text{Co}_{0.2}\text{Mn}_{0.3}\text{O}_2$, cathode material: towards the superior rate capability and cycling performance. *J Alloys Compd* 699:358–365
32. Wang D, Liu M, Wang X (2016) Facile synthesis and performance of Na-doped porous lithium-rich cathodes for lithium ion batteries. *RSC Adv* 6(62)
33. Chang ZR, Qi X, Wu F (2006) Preparation of co and Al coped LiNiO_2 cathode material by using eutectic mixed lithium salt with lower melting point. *Chem Eng* 34:50–53
34. Wu XW, Li YH, Xiang YH (2016) The electrochemical performance of aqueous rechargeable battery of $\text{Zn}/\text{Na}_{0.44}\text{MnO}_2$ based on hybrid electrolyte. *J Power Sources* 336:35–39
35. Su MR, Wan HF (2018) Multi-layered carbon coated Si-based composite as anode for lithium-ion batteries. *Powder Technol* 323:294–300